Aquatic Geochemistry **9:** 305–341, 2003.

Formation of Colloidal Silica and Alumina during Experimental Granodiorite Weathering

JIŘÍ FAIMON
Faculty of Sciences, Institute of Geological Sciences, Masaryk University, Kotlářská 2, 611 37 Brno, Czech Republic
E-mail: faimon@sci.muni.cz

(Received 18 March 2003; accepted 3 March 2004)

Abstract. The role of aluminum and silica in the formation of colloids during granodiorite weathering was studied on the basis of long-term experiments in batch reactors. Rock samples were dissolved in un-buffered solutions of initial pH $\sim$ 3.2, 5.4, and 9.9 at ambient conditions for 500 days. During weathering, extremely high supersaturation with respect to various secondary solids was attained in the solutions. Consequently, new solids, part of which was conserved in solutions as colloids, condensed. The mean concentrations of colloidal Si reached values of 70, 50, and 48 μmol 1^{-1} in the alkaline, neutral, and acid solutions, respectively. The mean concentrations of colloidal Al, reached values of 34, 22, and 12 μmol 1^{-1} in the alkaline, neutral, and acid solutions, respectively. The concentration of colloids gradually decreased after 200-400 days of experiment. This phenomenon was interpreted as being due to the competition between homogeneous nucleation and crystal growth. At the initial stages of the experiments, the colloidal species (predominantly colloidal Al) comprised a large proportion of the total amounts of aqueous species. Their share, however, decreased with time. The molar Al/Si-ratios of colloids were as high as 2–2.5 at the early stages of the experiment. After 250–300 days of experiments, on the other hand, these ratios decreased to values of about 0.5 in both the neutral and alkaline solutions and to a value of 0.15 in the acid solution. The evolution of colloids was consistent with the evolution of secondary solids in the sequence *Al-hydroxides – clay minerals (illite*, chlorite), in both the neutral and alkaline solutions. In acid solutions, the evolution of Al/Si-colloids was influenced by the presence of sulfate ion and Al-sulfate precipitation. Besides Al and Si, other elements, in particular Ca or Mg as a major component and Na, K, P, S, and Cl as minor components, readily participated in the formation of colloids.

Key words: aluminum, colloids, dynamics, granodiorite, silica, supersaturation, weathering

1. Introduction

Colloids are thought to be particles, which tend to remain dispersed in a medium. The diameter of such particles ranges from 1 to 1000 nm (e.g., Yariv and Cross, 1979; Mills et al., 1991). Some authors have shifted the upper limit of the diameter to as much as 10 μm (Stumm and Morgan, 1981; Puls and Powell, 1992). Other authors (Von Gunten et al., 1988; Waber

et al., 1990; Puls et al., 1990, 1991; Vilks et al., 1991) have occasionally used a different classification of aqueous constituents: soluble matter (molecules <l nm, colloidal particles <450 nm) and particulate matter (suspended particles >450 nm).

Natural colloids commonly include both inorganic macromolecules and organic macromolecules (polymers, fragments of solids, aggregates, and other objects of the cited dimensions). The role of natural colloids from the geological point of view is connected with the redistribution of elements in the earth's crust (1) and with environmental quality (2):

(1) Inorganic colloids, in addition to true solutions and coarse suspensions, take part in the fluxes of matter from primary rocks to secondary ones. The colloid particles of hydrated oxides, clay minerals, and others can aggregate (Overbeek, 1977; Stumm and Morgan, 1981; Hall et al., 1991) and participate in the formation of sediments and soils (Thornber et al., 1987).

(2) Colloids, due to high sorption ability and mobility in porous media, may serve as "pollutant carriers" (Degueldre et al., 1989; Means and Wijayaratne, 1982; Von Gunten et al., 1988; Waber et al., 1990; Mills et al., 1991; Puls et al., 1990, 1991; Vilks et al., 1991; Puls and Powel, 1992). They may operate, on the other hand, as "pollutant scavengers" as soon as they aggregate and settle together with the pollutants (Kühnel, 1987; Mills et al., 1991, Steinmann et al., 1999).

Little is known about the mechanism of colloid formation during weathering processes. There are two possible mechanisms:

1. The disintegration of primary grains into particles of colloidal dimensions, without any significant changes in their composition (except for surface hydration or hydrolysis). Some authors do not consider this mechanism very significant because of the increasing surface energy acting against this process (e.g., Yariv and Cross, 1979). Nevertheless, once formed and settled, aggregates of colloids can be re-dispersed by some processes that overcome inter-particle attractive forces, e.g., by kinetic energy of media (Lægdsmand et al., 1999, Missana et al., 2003) or by disintegration/dissolution of "cementitious phase" (Grindrod et al., 1999, Swartz et al., 1997).
2. The polymerization of the dissolved components and the condensation of colloid particles in supersaturated solutions.

Many investigators have shown that Al-hydroxides can be easily polymerized at neutral and alkaline pH levels (Bache and Sharp, 1976; Bottero et al., 1980; Bourrié et al., 1989; Moran and Moore, 1989). These polymers can grow into particles of colloidal dimensions. Si alone cannot be expected to form colloids because of the relatively high solubility of amorphous silica gels. The Si-concentration needed for polymerization exceeds by 4–10 times the equilibrium concentration of amorphous SiO_2, i.e. $10^{-2.7}$ mol l^{-1} (Rothbaum and Rohde, 1979; Crerar et al., 1981; Hunter, 1983). Such a high

value is at variance with the common Si-concentrations in aquifers. However, sufficient Si-concentrations can occur during the evaporation of solutions in soils. Recently, Dietzel (2000) mentioned that polysilicic acids could be directly evolved from weathered silicates. These polymers, however, consequently decomposed into monomeric species that were stable under experimental conditions.

In fact, silica together with aluminum is presumed to form amorphous aluminosilicate (Adu-Wusu and Wilcox, 1991; Holdren and Adams, 1982; Mackin and Aller, 1984; Wada and Wada, 1981; Yamanaka et al., 1986; Yokoyama et al., 1987, 1991). This probably occurs during Al-polymerization or before, by the formation of a soluble Si/Al-monomer (Browne and Driscoll, 1992). Similarly, soluble Ga/Si, Fe/Si, and even Cu/Si complexes in aqueous solutions were recently depicted by Pokrovski et al. (2002, 2003) and Yates et al. (1998), respectively.

Supersaturation, the essential condition for condensation of colloids, is often understood as the result of a temperature drop, pressure change, changes in chemical composition, or evaporation. However, supersaturation could also be a consequence of reaction kinetics, when the dissolution of primary phases occurs faster than the nucleation and growth of secondary phases (Lasaga, 1981). Metals such as Al, Fe, or even Ca, can easily reach high supersaturation with respect to their hydroxides, hydrated oxides, carbonates, sulfates, or fluorides (Degueldre et al., 1989; Klepetsanis and Koutsoukos, 1991; Vilks et al., 1991; Faimon and Ondráček, 1993).

The goal of this work was to find out whether Si/Al-colloids can be formed in a "*closed*" *rock*-water system (although open to atmosphere, without any mass fluxes of Si/Al from the surroundings) at constant conditions. One could expect that such systems will simply evolve toward equilibrium. However, this evolution (reaction path) could be connected with attainment of steady states, at which supersaturation with respect to various secondary phases is achieved. Consequently, processes such as polymerization and condensation are expected, during which a part of the new phase can be "conserved" in solution as colloids.

2. Experimental Methods

2.1. SAMPLES

Granodiorite from the Brno massif (type Brno-Řečkovice, Czech Republic) was chosen for weathering experiments. The rock sample was broken, ground, sieved through brass sieves as a water suspension, multiply washed with distilled water, and dried at 110 °C. Iron impurities (which result from grinding) were removed by a permanent magnet. The 70–90 μm size fraction

was used for the experiments. The purity and the size of the grains were checked by a scanning electron microscope (SEM – CamScan4-DV) coupled with EDXR spectrometry (LINK AN 10000). The granodiorite composition is reported in Tables I and II. Based on EDX analysis, it was found that plagioclase was constituted of albite, $Na_{0.93}Ca_{0.07}Al_{1.07}Si_{2.93}O_8$, and oligoclase, $Na_{0.73}Ca_{0.27}Al_{1.27}Si_{2.73}O_8$. The molar ratio of albite/oligoclase, 4.3, was computed. The majority of biotite identified on modal analyses was almost completely changed into chlorite of the average composition $Ca_{0.03}Mn_{0.04}Mg_{2.98}Fe_{1.95}Al[AlSi_3O_{10}](OH)_8$. Relatively fresh hornblende was of the average composition of $Na_{0.44}\ K_{0.20}\ Mg_{2.74}\ Ca_{1.97}\ Mn_{0.09}\ Ti_{0.16}\ Al_{1.19}[Al_{0.45}Si_{7.55}O_{22}](OH)_2$.

2.2. WEATHERING

Three runs, each of two parallel batch experiments, were performed: Hundred gram samples together with a solution volume of 1500 ml were placed in a plastic bottle and left to react at ambient conditions as an open system. Three types of un-buffered solutions were applied: acid (H_2SO_4, initial pH = 3.2), neutral (distilled water, initial pH = 5.4) and alkaline (NaOH, initial pH = 9.9). The reaction mixtures were briefly shaken every day.

2.3. THE ANALYSES OF SOLUTIONS

The pH of the solutions was measured weekly by a glass electrode SEO 212 (Sultech) combined with a pH-meter OP 2 (Radelkis Budapest). Approximately once every two months, 15-ml aliquots were pipetted out from the solutions. The solution was filtered through membrane filters (ME 28/41ST – 1.2 μm nominal pore size) to remove possible disintegrated primary grains and secondary precipitates, and to define the ''upper limit'' of the size of the colloid particles. The aliquots were analyzed for Al and Si by ICP–OES (UNICAM PU 7000). From some aliquots, polymers and colloids were separated.

2.4. THE SEPERATION AND ANALYSES OF COLLOIDS

Gel filtration chromatography (GFC) on Sephadex (G-50-150, Sigma Chemical Co, the separation range of 1500–30,000 molecular weight, standardized on globular proteins) was applied (Determann, 1967; Faimon and Ondráček, 1993; Yau et al., 1979). The GFC differs from the more commonly used gel permeation chromatography (Tarutani, 1970; Shimada and Tarutani, 1979; Crerar et al., 1981; Hine and Bursill, 1984) in the adjustment of a ''separating point''. This point was chosen to be the edge of the linear part of the ''separation characteristic'', which is the

Table I. The chemical composition of granodiorite

Methods	Components										Molar ratio		
	SiO_2 gm	$A1_2O_3$ cm	K_2O fph	Na_2O fph	CaO AAS	MgO AAS	FeO bch	Fe_2O_3 AAS	TiO_2 sph	MnO AAS	Al/Si	Na/Si	K/Si
Wt. %	71.86	15.14	2.97	4.76	1.66	0.79	0.70	0.92	0.26	0.01	0.248	0.128	0.053
Mol. %	67.06	16.65	3.54	8.61	1.16	1.10	0.55	0.65	0.18	0.01			

gm – gravimetry, cm – complexometry, fph – flame photometry, bch – bichromatometry, sph – spectrophotometry, AAS – flame atomic absorption spectrometry

Table II. The mineral composition of granodiorite

Phase	Composition		
	Stoichiometry[a]	Vol.%[b]	Mol.%[c]
Plagioclase			
Albite	$Na_{0.93}Ca_{0.07}Al_{1.07}Si_{2.93}O_8$	34.6	19.20
Oligolase	$Na_{0.73}Ca_{0.27}Al_{1.27}Si_{2.73}O_8$		4.50
Amphibole (hornblende)	$Na_{0.44}K_{0.20}Mg_{2.74}Mn_{0.09}Ca_{1.97}$-$Ti_{0.16}Al_{1.19}Al_{0.45}Si_{7.55}O_{22}(OH)_2$	18.4	4.78
Opaques (magnetite)	Fe_3O_4	5.0	7.72
Quartz	SiO_2	16.3	49.39
K-feldspar	$KAlSi_3O_8$	12.7	8.02
Chlorite	$Ca_{0.03}Mn_{0.04}Mg_{2.98}Fe_{1.95}Al_2$-$Si_3O_{10}(OH)_8$	7.0	2.28
Epidote	$Ca_{1.98}Na_{0.01}Fe_{0.94}Ti_{0.01}$ $Al_{2.06}Al_{0.01}Si_{2.99}0_{12}(OH)$	2.4	1.19
Biotite	$KMgAlSi_3O_8(OH)_2$	2.2	1.01
Titanite, Apatite	$CaTiSiO_5$	1.4	1.92

[a]EDX analyses.
[b]Modal analyses.
[c]Calculated.

plot of a detector response vs. elution volume (Determann, 1967). The solution passing the gel column was separated into two fractions: (1) monomeric (true solution) and (2) polymeric (colloidal). The experimental arrangement was similar to that which had been used by Crerar et al. (1981). The column size was 17 × 220 mm (V∼50 ml). A 10-ml sample was applied for separation; distilled water was used as an eluent. The elution volume of the colloids was between 20 and 40 ml (for details, see Faimon and Ondráček, 1993; Faimon, 1995). The column efficiency, checked by standard solutions, was better than 95%. The "colloid fraction" from the GFC was analyzed by ICP/OES for Al and Si.

Some parts of the colloid fractions were evaporated almost completely under an infra-radiator. The concentrate was dropped into a sample carrier (graphite target), dried, vacuum coated with gold and graphite, and studied by SEM and EDXA methods (electron microprobe, Cameca, SX100), respectively. After termination of the experiments, solutions were left to freely evaporate to dryness at ambient conditions. Then, the crust covering a layer of primary grains was separated and re-dispersed in distilled water in an ultrasonic bath. Suspensions/dispersions of secondary solids/colloids were

isolated from the admixed grains of primary phases by decantation. The solids and colloids were studied by the former methods.

2.5. COMPUTING, MODELING

Geochemical modeling was based on the PHREEQC computer code (Parkhurst and Appelo, 1999). Saturation indexes (SI = log Q/K, where Q is the reaction quotient and K is the solubility product) were calculated from aqueous concentrations after subtracting colloidal Si and Al. All other computations and data evaluation were performed using the program MS Excel.

3. Results

3.1. SOLUTIONS

The evolution of pH and aqueous concentrations of Si, Al, K, and Na during experiments is presented in Figure 1.

3.1.1. *pH*

Significant changes in pH took place during the initial stages of the experiments (Figure 1, the upper graph). The pHs of acid solutions quickly increased from the initial value of pH = 3.2 to the limiting value of about pH $\sim$ 4.5. Similarly, the pHs of nearly neutral solutions increased from the initial value of pH = 5.4 to a value of about pH$\sim$7.3. The pHs of alkaline solutions, on the other hand, decreased from the initial value of pH = 9.9 to the limiting value of about pH $\sim$ 7.5.

3.1.2. *Silica*

The concentrations of aqueous silica increased sharply at the initial stages of the experiments. Thereafter, the concentrations slowly increased, as if towards a steady state/equilibrium (Figure 1). The highest Si-concentration was reached in neutral solutions, [Si] $\sim$ 750 μmol l^{-1}. In acid and alkaline solutions, the Si-concentrations reached a value of about 450 μmol l^{-1}, and they seemed to be nearer the steady state.

3.1.3. *Aluminum*

The aqueous concentrations of aluminum in acid solutions quickly reached a limiting value of about 10 μmol l^{-1}. In alkaline and neutral solutions, on the other hand, the Al-concentrations reached extremely high values of up to 160 and 290 μmol l^{-1} , respectively (Figure 1).

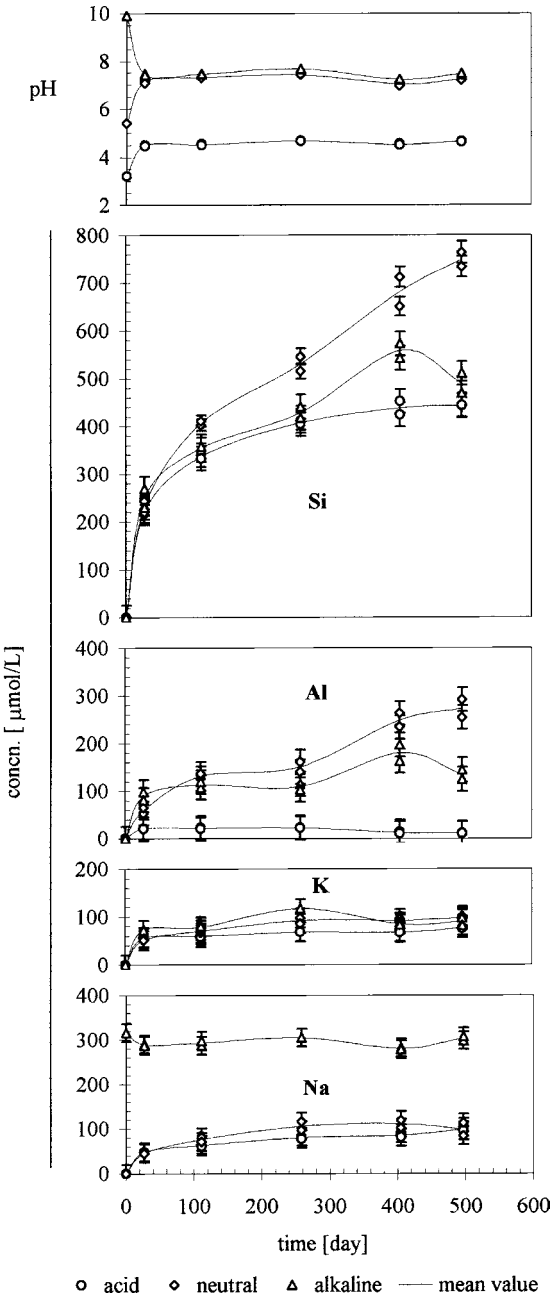

Figure 1. Evolutions of pH and concentrations of aqueous species.

3.1.4. *Potassium and sodium*

Both concentrations of aqueous K and Na quickly approached the limiting values of about 70–100 μmol l^{-1} (Figure 1). The high Na-concentration in

the alkaline solutions was a result of addition of NaOH to adjust the pH-value at the start of the experiments. The initial value, 316 μmol l^{-1} slightly decreased to 280–300 μmol l^{-1} at the final stages of the experiment.

3.1.5. *The supersaturation of solutions*

The high supersaturation with respect to various secondary solids was achieved in all solutions (Figure 2). In particular, the supersaturation with respect to K-mica, Na-beidellite, kaolinite, and pyrophyllite in the neutral and alkaline solutions was enormous (SI $\sim$ 7–16). In acid solutions, on the other hand, the supersaturation with respect to these phases was significantly lower (SI $\sim$ 1–5). The supersaturation was stable or increased with time, except for a very slight decrease between 400 and 500 days in the neutral and alkaline solutions, and between 250 and 300 days in the acid solutions. The undersaturation with respect to primary silicates (K-feldspar and albite) was kept only in the acid solutions.

3.2. COLLOIDS

The total concentrations of colloidal Si and Al in solutions are presented in Figure 3. These concentrations increased sharply in the alkaline solutions and more gradually in the neutral and acid solutions. They reached a maximum during the period from the 200th to 400th day, and then decreased to near zero at about the 500th day of the experiment.

The relatively high data scattering is probably a result of (l) the little bit "different evolution" of parallel experiments (the weathering processes as dissolution, nucleation, and crystal growth are extremely complex and hardly reproducible) and (2) errors resulting from the separations and analytical determinations.

The colloidal Si reached a concentration of 71 and 66 μmol l^{-1} (the maximal mean values were 69 and 50 μmol l^{-1}) in the alkaline and neutral solutions, respectively. In the acid solution, one value of the Si-concentration reached 63 μmol l^{-1}. The maximal mean value was 48 μmol l^{-1}.

The highest concentration of colloidal Al, nearly 37 μmol l^{-1}, was reached in the alkaline solutions. The mean concentrations of colloidal Al reached the maximal values of 34, 22, and 12 the μmol l^{-1} in the alkaline, neutral, and acid solutions, respectively.

SEM observation during the course of experiments showed that the colloidal matter consisted of a superfine fraction and spherical particles as large as 1 μm diameter. The composition of the particles was highly variable. For example, the typical composition of the particles separated from alkaline solution on the 139th day of the experiment (based on EDX-analyses) is

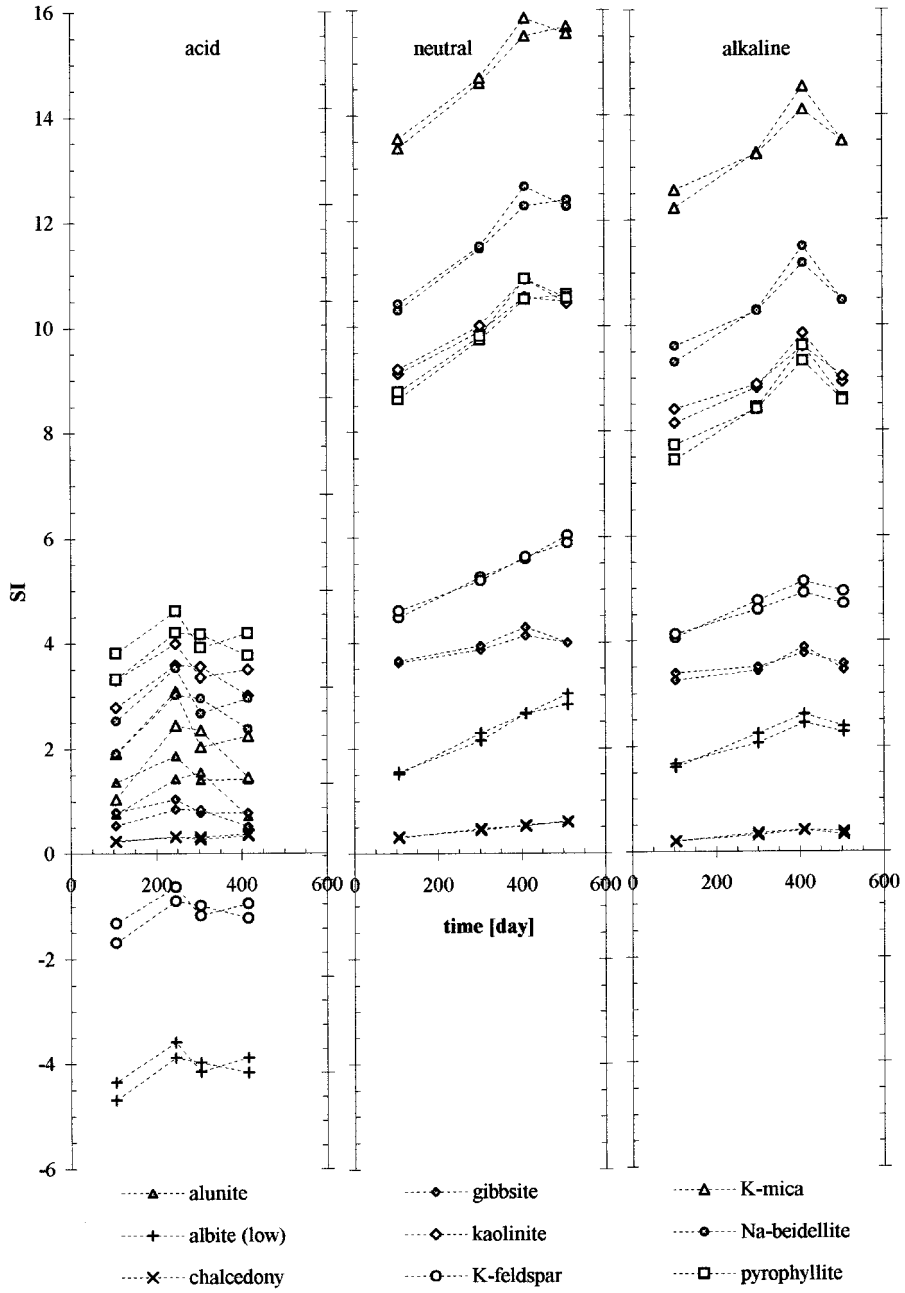

Figure 2. Evolution of supersaturation with respect to selected phases. Based on PHREEQC code (Parkhurst and Appelo, 1999).

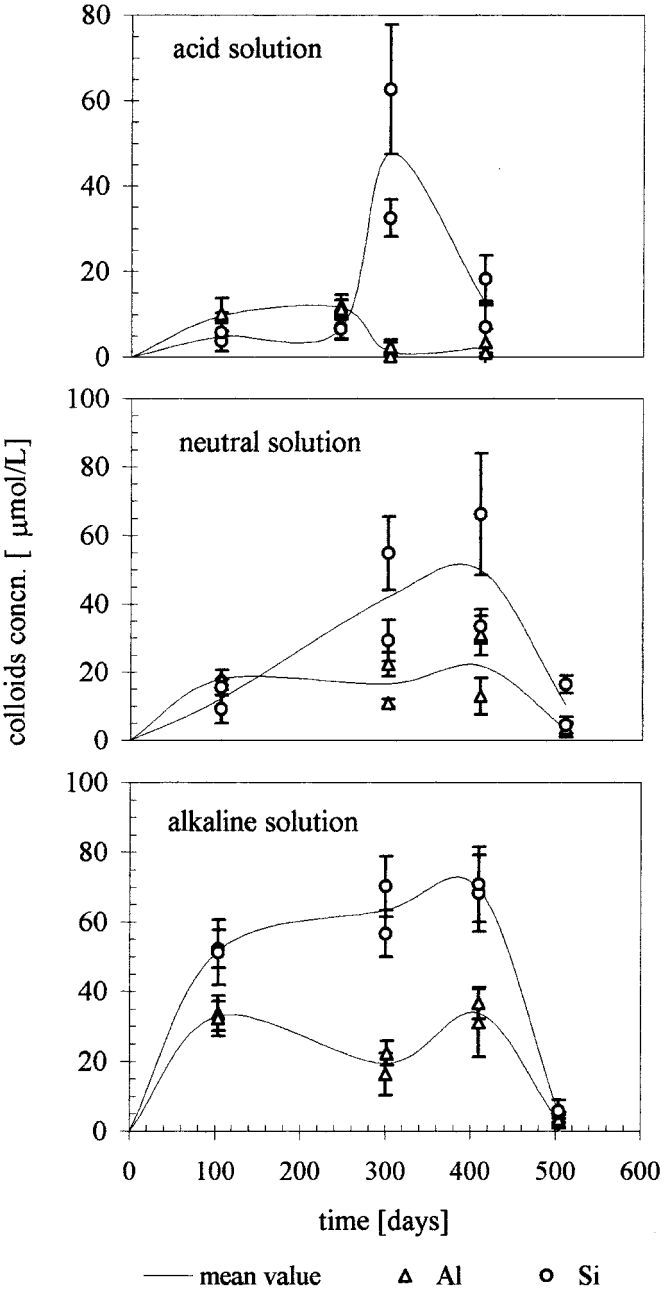

Figure 3. Evolution of the concentrations of colloidal Si and Al.

shown in Figure 4. In addition to the high contents of silica and alumina, an extremely high content of calcium is apparent. Elements that have been minor in granodiorite (P, S, and Cl) are slightly concentrated. Next to this

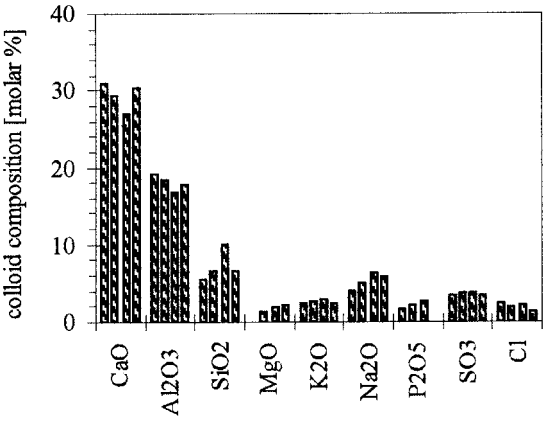

Figure 4. Composition of the colloid particles separated from basic solution on the 139th day of the experiment (based on EDX-analyses).

Table III. Average composition[a] of the colloids formed in solutions

Components [mol %]	Solution					
	Acid		Neutral		Alkaline	
	1	2	1	2	1	2
Na_2O	4.46	2.73	4.11	4.27	3.77	2.84
MgO	26.78	16.83	7.09	6.60	7.59	5.62
$A1_2O_3$	7.07	9.91	13.70	13.50	14.85	12.79
P_2O_5	0.06	0.12	0.07	0.11	0.12	0.03
Cl	1.76	1.64	0.43	0.40	0.48	0.08
K_2O	2.59	2.03	1.89	2.13	2.97	3.01
CaO	3.99	0.75	4.75	4.90	4.72	2.13
TiO_2	1.56	0.24	0.80	1.07	0.99	1.47
MnO	3.75	1.69	0 15	0.24	0.40	0.13
FeO	4.28	5.48	8.71	6.30	8.38	9.17
BaO	0.03	0.01	0.04	0.04	0.04	0.01
SiO_2	22.71	37.75	57.88	59.92	55.45	62.66
SO_3	20.97	20.82	0.36	0.52	0.23	0.05

[a]EDX analysis, electron microprobe, spot size 50 μm.

composition, the part of colloidal matter consisted of almost pure alumina (calcium was identified as a very minor element).

The final composition of the colloids re-dispersed from the settlings obtained after the finish of the experiments is presented in Table III. In the colloidal mater formed in alkaline and neutral solutions, silica and alumina were dominant, whereas Mg and Fe contents were somewhat lower. Other

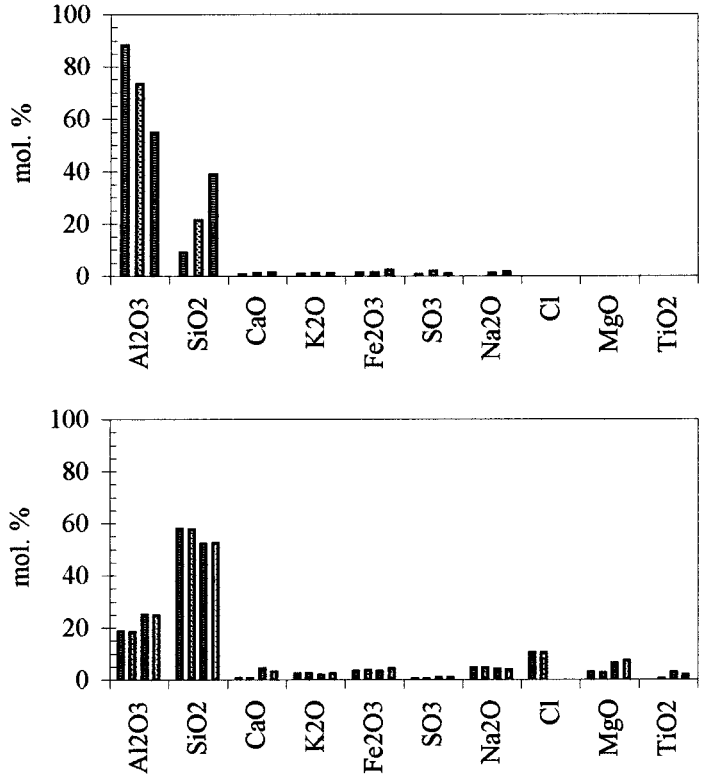

Figure 5. Composition of the secondary solids isolated from the neutral solutions on the 24th day of the experiment (based on EDX-analysis).

elements such as Na, K, and Ca were minor. In the colloids formed in acid solutions, on the other hand, silica, magnesium and sulfur were dominant. Al-content was somewhat lower. Other elements such as Na, K, Ca, Ti, Mn, and Fe were minor. In all colloids, slightly enhanced contents of P, Cl and Ba were recognized.

3.3. SECONDARY PHASES

The secondary phases formed at the early stages of the experiments were largely enriched in alumina. The composition of the solids isolated from the neutral solutions on the 24th day of the experiment (based on EDX analysis) is presented in Figure 5. In addition to the dominant aluminum, silica occasionally appeared as another component (see the upper graph). Other elements were minor. In few single phases, the silica contents exceeded that of alumina (see the lower graph).

The secondary phases gathered after experiments were very fine-grained, and there was difficulty in determining single phases. Therefore, based on

Table IV. Average composition[a] of the secondary phases formed in solutions

Components [mol. %]	Solution					
	Acid		Neutral		Alkaline	
	1	2	1	2	1	2
Na_2O	1.08	1.73	1.00	1.23	1.13	1.00
MgO	3.66	4.06	2.96	8.33	3.13	5.19
$A1_2O_3$	13.73	11.56	23.32	15.26	12.68	13.11
P_2O_5	0.11	0.02	0.04	0.04	0.09	0.03
Cl	0.08	0.03	0.03	0.09	0.11	0.02
K_2O	5.06	3.80	6.17	3.66	3.54	9.61
CaO	6.04	2.14	1.19	1.71	0.20	1.05
TiO_2	1.09	0.99	0.26	0.67	1.67	0.36
MnO	0.14	0.15	0.07	0.40	0.00	0.18
FeO	7.21	7.03	3.06	11.64	19.94	3.74
BaO	0.11	0.03	0.03	0.04	0.04	0.04
SiO_2	58.26	67.89	61.81	56.79	57.38	65.61
SO_3	3.44	0.55	0.07	0.14	0.11	0.08

[a]EDX analysis, electron microprobe, spot size 50 μm.

microprobe analysis of large spot sizes (EDX-analysis), just average compositions were determined (Table IV). Silica and alumina were dominant in all solids. In addition, the content of Mg, K, and primarily of Fe was high. Slightly enhanced contents of calcium and sulfur were visible only in the solids isolated from the acid solutions. The minor/trace elements in granodiorite, Ti, P, Cl, Ba, and S, were slightly concentrated in all secondary phases.

Based on X-ray diffraction, chlorites (clinochlore, chamosite), K-mica and small contents of other phases (quartz, diaspore and carbonate) were identified in the secondary phases isolated from the alkaline and neutral solutions after evaporation. In the secondary solids formed in the acid solutions, on the other hand, only sulfates were recognized. All phases found are summarized in Table V.

4. Discussion

4.1. DISSOLUTION

4.1.1. *pH*

The changes in pH at the initial stages of the experiment (Figure 1) were the result of a cumulative effect of alkalinity increase during granodiorite dis-

Table V. Secondary minerals identified by x-ray diffraction

Mineral	Formula
Acid solution	
Zaherite	$Al_{12}(SO_4)_5(OH)_{26} \cdot 20H_2O$
Kieserite	$MgSO_4 \cdot H_2O$
Sodium alum	$NaAl(SO_4)_2 \cdot 12H_2O$
Neutral Solution	
Clinochlore	$(Mg,Fe)_6(Si,Al)_4O_{10}(OH)_8$
Chamosite	$(Fe,Al,Mg,Mn)_6(Si,Al)_4O_{10}(OH)_8$
Magnesian Chamosite	$(Fe_{2.8}Mg_{1.8}Al)(Si_{2.8}Al_{1.2})O_{10}(OH)_8$
Muscovite	$(K,Na)_{0.75}(Al,Mg)_2(Si,Al)_4O_{10}(OH)_2$
Quartz	SiO_2
Alkaline Solution	
Clinochlore	$(Mg,Fe)_6(Si,Al)_4O_{10}8$
Diaspore	$Al_2O_3 \cdot H_2O$
Quartz	SiO_2
Ankerite	$Ca(Mg_{0.67}Fe_{0.33})(CO_3)_2$
Muskovite	$(K,Na)_{0.75}(Al,Mg)_2(Si,Al)_4O_{10}(OH)_2$

solution and buffering by atmospheric CO_2. The pH changes were verified by modeling using the PHREEQC code: during a virtual dissolution of 1×10^{-3} mol of the rock composed of 53, 12, 13, 22 mol% of albite, oligoclase, hornblende, and K-feldspar (i.e., analogical to sample) at $p_{CO_2} \sim 10^{-3}$ atm, the pH of the solution changed from the initial values of 3.2, 5.4, 9.9 to about 4.5, 7.2, 7.8, respectively.

4.1.2. *Composition of solutions*

In general, kinetics controls to what extent a single phase will contribute to aqueous species. Next to plagioclase, mainly hornblende, biotite, epidote and K-feldspar participates in aqueous concentrations (Sverdrup and Warfvinge, 1995). Chlorite and quartz do not seem to be very significant due to their lower dissolution rates. The rate constants quantifying the release of Si from silicates into solution are summarized in Table VI.

4.1.2.1. *Al/Si stoichiometry*. In the neutral and alkaline solutions, the average Al/Si-ratios varied between 0.26 and 0.36 (Figure 6). These values are higher than the average Al/Si-stoichiometry of granodiorite, 0.25, but somewhat lower than the Al/Si-stoichiometries of albite and oligoclase, 0.37 and 0.47, respectively. This indicates dissolution of alternative phases in addition to

Table VI. Experimentally determined rates of silicate dissolution

Silicate	*p*H	*T* °C	Si release rate log [mol m^{-2} s^{-1}]	Authors
Hornblende	6.8-7.4	ac	−10.96	Kalinowski et al. (2000)
Hornblende	nn	ac	−11.8	Liermann et al. (2000)
Hornblende	4	25	−11.9	Zhang and Bloom (1999)
Epidote	4.05	25	−11.72	Kalinowski et al. (1998)
Epidote	6.5	25	−11.93	Kalinowski et al. (1998)
Biotite	3-8	25	−11.05	Malmström and Banwart (1997)
Biotite	3	25	−11.6	Taylor et al. (2000)
Albite	6	ac	−11	Welch and Ullman (1996)
Albite	5	ac	−11.1	Holdren and Speyer (1985)
Albite	5.6	25	−12.0	Hamilton et al. (2000)
Albite	5	ac	−12.1	Knaus and Wolery (1986)
Oligoclase	5	ac	−11.4	Mast and Drever (l987)
Oligoclase	5.4	ac	−11.6	Stillings et al. (l996)
Oligoclase	5	ac	−12	Oxburg et al. (1994)
K−feldspar	5	ac	−11.1	Holdren and Speyer (1985)
Orthoclase	5	ac	−12.3	Busemberg and Clemency (1976)
Microcline	5.6	ac	−12.8	Schweda (l989)
Chlorite	5.3	25	−11.96	Brandt et al. (2003)
Chlorite	7.7	ac	−12.46	Rochelle et al. (l996)
Chlorite	5	ac	−12.52	May et al. (1995)
Quartz	nn	25	−14.12	Gíslason et al. (1997)
Quartz	nn	25	−14.51	Rimstidt and Barnes (1980)

Note: nn – near neutral, ac – ambient conditions.

plagioclases. The Al/Si-ratios slightly increased with a slope of 2×10^{-4} day^{-1} in the neutral solutions and decreased with a slope of -1.3×10^{-4} day^{-1} in the alkaline solutions. Provided dissolution rate of single phase is constant, the evolution of the aqueous Al/Si-ratio indicates a selective precipitation of Al-Si phases of a different stoichiometry when compared with the primary minerals.

In the acid solutions, the Al/Si-ratio was extremely low and gradually decreased from 0.09 to 0.02. Because the dissolution rates are similar in alkaline and acid solutions (as document Si-concentrations, see Figure 1), the low value of Al/Si-ratio indicates a large precipitation of Al-rich phases. This is somewhat surprising when compared with alumina behavior in the neutral and alkaline solutions. However, the high sulfate concentration (due to the initial addition of sulfuric acid to adjust pH) in the acid solutions could be

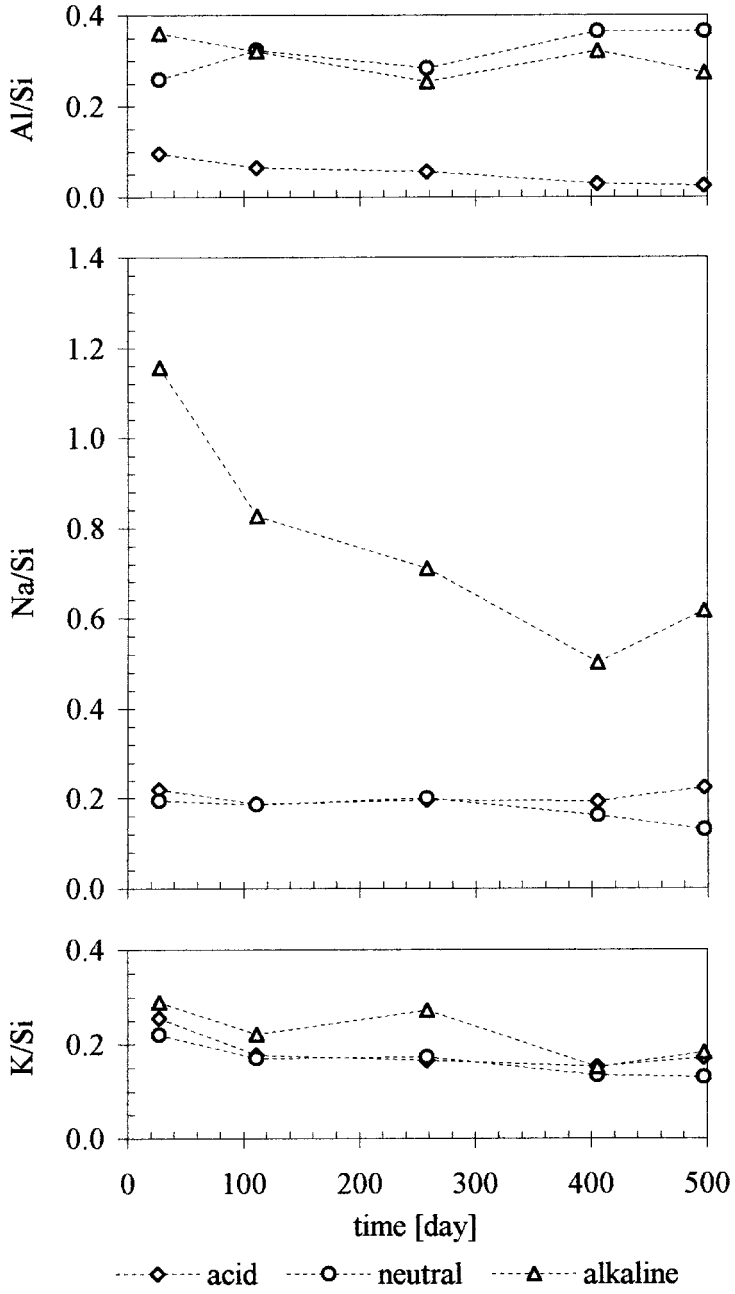

Figure 6. Evolution of the basic average stoichiometries in the solutions.

responsible for the precipitation of alumina-sulfates. For example, the positive values of saturation index (SI $\sim$ 0.72–1.87) indicate the possibility of precipitation of alunite, $KAl_3(SO_4)_2(OH)_6$.

4.1.2.2. *Na/Si-stoichiometry*. Plagioclase and hornblende are the potential sources of aqueous Na (see Table II). In the acid solutions, Na/Si-ratios were roughly constant (0.19–0.22, 0.20 on average). In the neutral solutions, Na/Si-ratios slightly decreased (from 0.20 to 0.13) (Figure 6). These values are significantly lower than the Na/Si-ratios 0.27 and 0.32 in oligoclase and albite, respectively. This suggests that (1) other phases contributed to aqueous silica and/or (2) some phases enriched in Na precipitated. In the alkaline solutions, the high initial Na/Si-ratio, 1.16, (the result of sodium hydroxide addition to adjust pH at the start of the experiment) decreased to 0.50–0.62. Such behavior is predominantly an effect of the large increase of aqueous silica contents. However, the slight decrease in the total Na-content with the slope of -0.017 μmol day^{-1} (Figure 1) suggests that it can be the result of Na-rich phase precipitation. The extremely high supersaturation with respect to Na-beidellite (SI $\sim$ 9.30–11.50) stresses this assumption. However, neither smectites nor the significantly enhanced content of sodium in the final secondary solids was found (see Table IV). Therefore, based on the supersaturation with respect to albite (SI $\sim$ 1.60–2.61), even the growth of primary solids (albite) should be considered.

4.1.2.3. *K/Si stoichiometry*. Despite a small content in granodiorite, biotite seems to be a potential source of aqueous potassium due to its relatively high dissolution rate (Table VI). In the acid solutions, the negative value of saturation index and the relatively high value of dissolution rate constant (Table VI) indicate that an additional source of potassium could be K-feldspar. In the neutral and alkaline solutions, on the other hand, the positive value of saturation index with respect to K-feldspar (SI $\sim$ 4.06–6.03) permits us to consider a growth of the primary mineral. The K/Si-ratios decreasing with a slope -1.5×10^{-4}, -1.7×10^{-4} and -2.3×10^{-4} day^{-1} (Figure 6) in the acid, neutral, and alkaline solutions, respectively, and the high supersaturation with respect to K-mica (SI $\sim$ 1.40–15.85), signalize that some K-clay minerals can precipitate (e.g., illite).

4.1.3. *Supersaturation*

The supersaturation of solutions was understood to be a consequence of the dynamics between the irreversible dissolution of primary minerals and the precipitation of secondary solids. All main possible processes in system *rock*-solution-secondary solids are depicted in a conceptual model (Figure 7). It consists of the reservoirs of primary solid A, solution B, secondary solid C, nuclei, and colloids. The arrows denote the fluxes of a *k*-component. The instantaneous aqueous concentration of the *k*-component is a result of operating of the overall flux $j^{(k)}_{o(sol)}$ of the *k*-component into solution is $j^{(k)}_{o(sol)} = \sum_i j_i^{(k)}$, where $i = 1$–6. At steady state, the overall flux $j^{(k)}_{o(sol)}$ is zero,

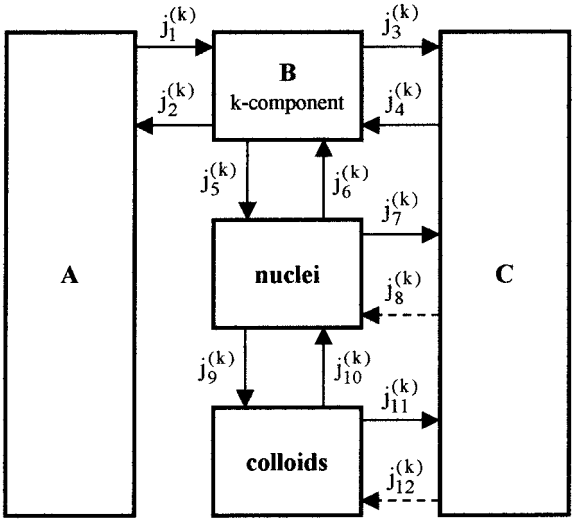

Figure 7. Conceptual box model of the *rock-water* interaction. A, B, and C are the reservoirs of primary rock, dissolved component, and secondary solids, respectively. The single arrows denote an *i*-flux of *k*-component, $j_i^{(k)}$. The dashed arrows express problematic fluxes.

$\sum_i j_i^{(k)} = 0$. If the flux $j_1^{(k)}$, is not balanced by flux $j_2^{(k)}$ (mineral A is far from equilibrium), the flux $j_1^{(k)}$"feeds" the solution by the *k*-component. Then, the instantaneous *k*-concentration can exceed the equilibrium *k*-concentration with respect to the phase $C^{(k)}$, and the solution is supersaturated.

4.1.4. *Individual fluxes*

The overall flux of the *k*-component into solution, $j_{o(sol)}^{(k)}$, is given by

$$j_{o(sol)}^{(k)} = dn^{(k)}/dt, \tag{1}$$

where $dn^{(k)}/dt$, is the total transfer of *n*-moles of the *k*-component into solution in time *t*.

The data sets on dissolution were regressed by the exponential function

$$c^{(k)} = \frac{a^{(k)}}{b^{(k)}}\left(1 - e^{-b^{(k)}t}\right) + d^{(k)}, \tag{2}$$

Where $c^{(k)}$, is the concentration of the *k*-component; $a^{(k)}$, $b^{(k)}$, and $d^{(k)}$ are "parameters" of the function. Equation (2) was found to be a somewhat modified result of the mathematical solution of the conceptual model (Figure 7) in which the fluxes $j_1^{(k)}$ *and* $j_3^{(k)}$ were solely considered. The steep increase in concentrations at the initial stages of experiments was attributed to a rapid dissolution of "new surfaces" (high energy surface sites, highly

strained areas on large grains and ultrafine particles as an artifact of sample preparation, see Wegner and Christie, 1983; Chou and Wollast, 1984; Brantley et al., 1986; Lasaga and Blum, 1986; Eggleston et al., 1989; Faimon, 1998). These data (between zero time and the 27th day) were inconsistent with the exponential dependency (Equation 2) and were regressed by linear function

$$c^{(k)} = p^{(k)}t + q^{(k)}, \tag{3}$$

where $p^{(\mathrm{k})}$ and $q^{(\mathrm{k})}$ are parameters of the function.

The overall flux of the k-component into the solution, $j^{(k)}_{\mathrm{o(sol)}}$ was calculated from the derivative of the regression functions

$$\frac{\mathrm{d}c^{(k)}}{\mathrm{d}t} = \frac{1}{V}\frac{\mathrm{d}n^{(k)}}{\mathrm{d}t} = \frac{1}{V}j^{(k)}_{\mathrm{o(sol)}}, \tag{4}$$

where V is the Volume of the solution, The derivation of Equations (2) and (3) gives

$$\frac{\mathrm{d}c^{(k)}}{\mathrm{d}t} = a^{(k)}\mathrm{e}^{-b^{(k)}t} \tag{5}$$

and

$$\frac{\mathrm{d}c^{(k)}}{\mathrm{d}t} = p^{(k)}, \tag{6}$$

respectively. The overall fluxes as a function of time are presented in Figure 8. The steep decrease of the flux between the 0th and 27th days is a consequence of the weakening of the flux from the new surface and the increase of the fluxes into secondary solids (nuclei/colloids). It seems reasonable to assume that the fluxes $j^{(k)}_2$, $j^{(k)}_3$, $j^{(k)}_4$, $j^{(k)}_5$, and $j^{(k)}_5$ are negligible at the start of dissolution. Thus, the single flux from rocks, $j^{(k)}_1$, was estimated by the extrapolation of Equation (5) to zero time. This operation allowed exclusion of the fluxes from new surfaces between the 0th and 27th days. The fluxes found $j^{(\mathrm{Al})}_1$ and $j^{(\mathrm{Si})}_1$ are summarized in Table VII. As can be seen, the fluxes into acid and alkaline solutions exceeded the fluxes into neutral solutions. This is consistent with the known tendency of silicate to dissolve at higher rates in acid and alkaline environments (see, e.g., Sverdrup and Warfvinge, 1988). The $j^{\mathrm{Al}}_1/j^{\mathrm{Si}}_1$ ratios are somewhat higher when compared with the aqueous Al/Si-ratios. This signalizes that the fluxes $j^{(\mathrm{Al})}_1$ are probably overstated. The non-negligible fluxes $j^{(\mathrm{Al})}_3$ with respect to $j^{(\mathrm{Al})}_1$ (in acid solutions especially due to alunite precipitation) could be the reason. The flux

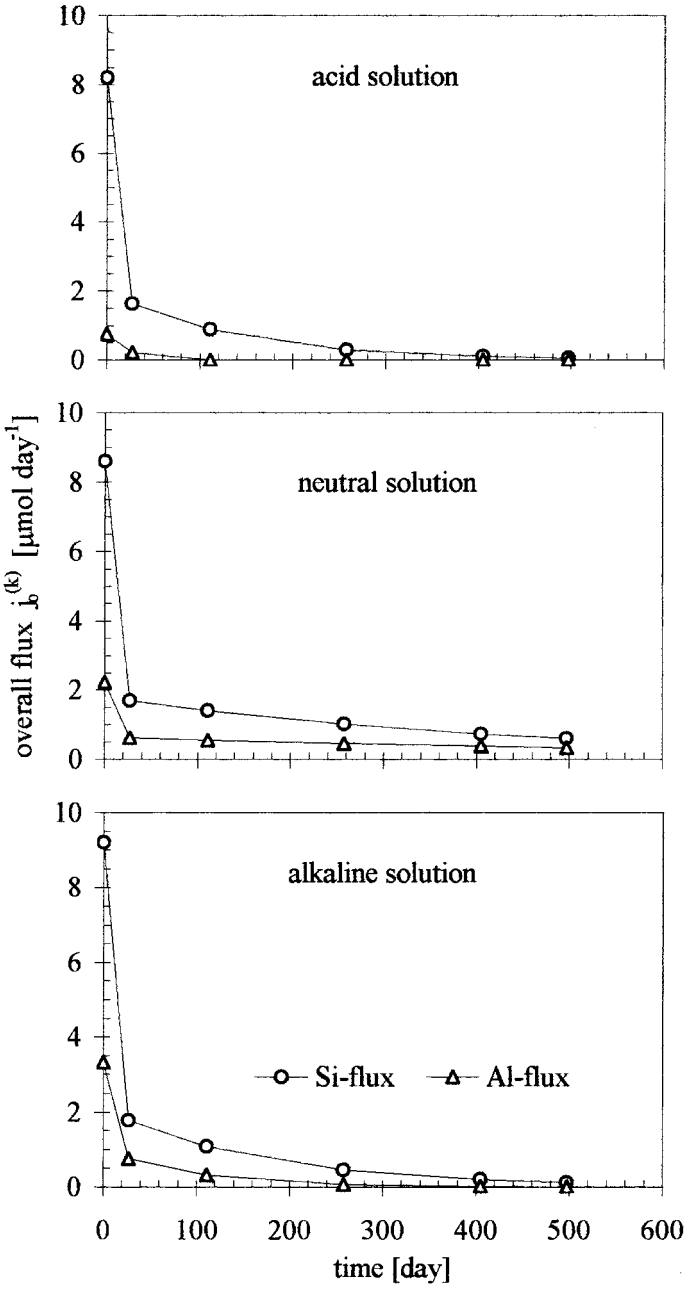

Figure 8. The overall Al- and Si-fluxes into the solutions as a function of time.

recalculated to unit surface area was understood as a rate constant of releasing of individual components. The rate constant of the release of Si from granodiorite into neutral solutions, $10^{-11.03}$ mol m^{-2} s^{-1} is in a lower

Table VII. Individual fluxes from granodiorite and the rate constants of single element releasing

	Solution		
	Acid	Neutral	Alkaline
$j_1^{(Si)}$ [μmol day^{-1}]	1.99	1.81	2.07
$j_1^{(Al)}$ [μmol day^{-1}]	0.91	0.64	0.99
$j_1^{(Al)}/j_1^{Si}$	0.46	0.35	0.48
k_{si} [mol m^{-2} s^{-1}]	$10^{-10.99}$	$10^{-11.03}$	$10^{-10.97}$
k_{Al} [mol m^{-2} s^{-1}]	$10^{-11.33}$	$10^{-11.48}$	$10^{-11.29}$

range of the values for Si-releasing from various silicates found by other authors based on laboratory experiments (Table VI). Predictably, on the other hand, the value $10^{-11.03}$ mol m^{-2} s^{-1} is significantly higher than the constants found on the basis of field mass balances.

4.2. COLLOID FORMATION

4.2.1. *Concentrations*

The maximal concentrations of the Al/Si colloids recorded in this work slightly exceeded those commonly referred for surface and ground waters. Viers et al. (1997) reported 7–12 and 0.4–l.l μmol l^{-1} (fraction 5 kDa–0.22 μm) of colloidal Si and Al, respectively, in "clear" tropical waters derived from laterites and granitic parents rocks (sampled from springs and shallow wells). These authors found somewhat higher concentrations, 4–20 and 6–16 μmol l^{-1} of colloidal Si and Al, respectively, in "color" organic-rich surface waters of the same region. Benedettia et al. (2002) proposed 10.6 and 2.9 μmol l^{-1} (fraction 5 kDa–0.22 μm) of colloidal Al in the Rio Negro and Amazon Rivers, respectively. Dupre et al. (1999) determined 40.2 μmol l^{-1} of colloidal Al, but only 1 μmol l^{-1} of colloidal Si (fraction 5 kDa–0.20 μm) in the organic-rich river waters draining granitic parental rocks in tropical forests. Dia et al. (2000) found up to 5 μmol l^{-1} (fraction 5 kDa–0.2 μm) of colloidal Al in groundwater of the shallow wells in the sediments developed on Proterozoic schists. In boreal rivers and their estuaries, Pokrovski and Schott (2002) found even lower concentrations: The waters in contact with granitoids (granites and granodiorites) showed 0.5–3.9 and 0.3–6 μmol l^{-1}, the waters draining other silicates (gneisses, amphibolites, sandstones, quartzites) exhibited 0.5–1.8 and 0.3–1.5 μmol l^{-1} and the water derived from other rocks (clays and limestones) contained 1.8–4.6 and 0.3–2.5 μmol l^{-1} of colloidal Si and Al (all in the fractions 1 kDa–0.8 μm), respectively. Porcelli et al. (1997), on the other hand, found up to

28.5 μmol l^{-1} of colloidal Si (fraction 3 kDa–0.45 μm) in the boreal rivers that had drained mica schitsts, quartzites, and amphibolites. Wilkinson et al. (1997) reported about 11 μmol l^{-1} of colloidal Si and 5 μmol l^{-1} colloidal Al (fraction 5 nm–5 μm) in a small eutrophic lake.

In contrast, higher concentrations of up to 64–172 and 19–131 μmol l^{-1} of colloidal Si and Al, respectively, were reported by McCarthy and Shevenell (1998) in the wells in fractured shale and karstic formations. Extremely high concentrations of up to 1500 μmol l^{-1} of colloidal Si and 12,000 μmol l^{-1} of colloidal Al (fraction 3 kDa–100 kDa) were found by Zänker et al. (2002) in the acid Fe-SO_4-rich water draining clays impregnated with sulfide ores.

The proportions of colloidal Al and Si to the total Al and Si contents are presented in Figure 9. The total aluminum consisted almost completely of colloidal aluminum in both the alkaline and neutral solutions on the 100th day of the experiment. In the acid solutions, Al-colloids represented up to 50% of the total Al. In all the solutions, the proportion of colloidal Al decreased with time. This behavior confirms the tendency of Al that largely entered into colloidal during the early stages of the experiment. The total Si included maximally 25% of colloidal Si. This can be due to differences in the Al/Si-stoichiometries of primary minerals and colloids. If the Al/Si-stoichiometry is 1/3 in primary minerals (e.g. plagioclase and K-feldspar) and 1/1 or 1/2 in colloids (as in kaolinite or smectites, respectively), some silica must remain "conserved" in solution. The concentration of such silica will finally be controlled by Si-amorphous gel solubility.

4.2.2. *Composition*

The activity diagram in Figure 10 shows that the system *granodiorite -water* mostly occur in the stability field of kaolinite. At the earliest stages of the experiment, however, the reaction paths probably crossed the stability field of gibbsite, at least in the neutral and alkaline solutions. This is consistent with the presumed Al-phase stability. At the later stages, when the concentration of silica and cations had increased, reaction paths moved into the pyrophyllite field representing smectite/illite in the model. Therefore, there is a good reason to assume that the colloidal matter evolves in a succession *gibbsite-kaolinite-smectite/illite* (or, at least, the precursors of such minerals; see, Steefel and Van Cappellen, 1990).

The evolution of the Al/Si-stoichiometries of colloids is shown in Figure 11. In the neutral and acid solutions, a high Al/Si-molar ratio of colloids was achieved at the early stages of the experiment, which is consistent with the occurrence of Al-rich solids. In the alkaline solutions, the Al/Si-ratio was almost constant, aside from somewhat elevated values at the early stages of the experiment. At the later stages, the Al/Si-ratio neared the value of 0.5, both in

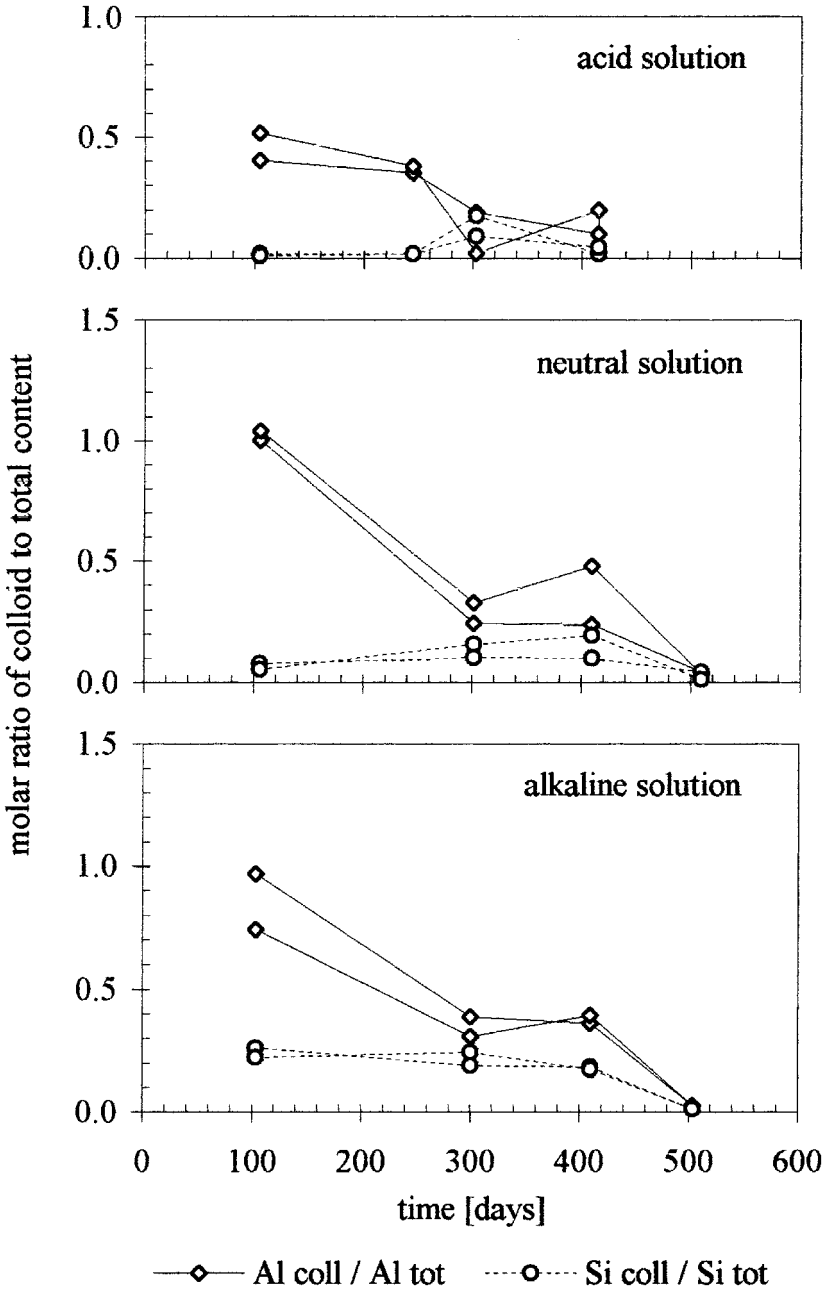

Figure 9. Proportion of the colloidal Al and Si to their total contents as a function of time.

the alkaline and neutral solutions. This stoichiometry indicates the existence of smectite/illite. Despite the high Al-fluxes out away from the acid solutions, the low final Al/Si-ratio of colloids, 0.15, signalized the poor tendency of Al that

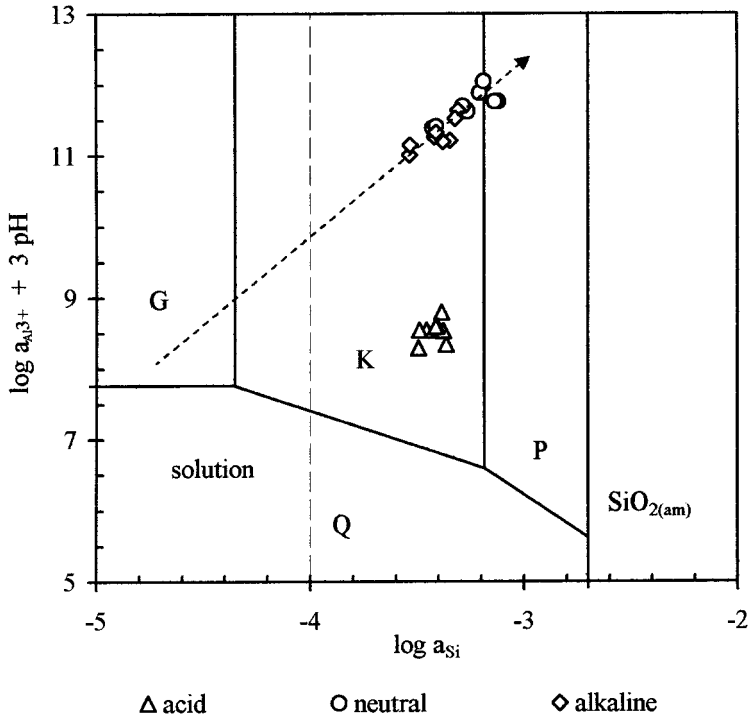

Figure 10. Al–Si–H2O activity diagram. The marks G, K, Q, P, and $SiO_{2(am)}$ symbolize gibbsite, kaolinite, quartz, pyrophyllite, and amorphous silica, respectively. The dashed arrow demarks a reaction path of rock-water system in the neutral and alkaline solutions. Experimental data were converted to activities on the basis of the PHREEQC code (Parkhurst and Appelo, 1999).

entered the colloids under these conditions. This can be explained by the high aggregation rate of Al-SO_4-phases (the relatively low pH value supports this idea) and, consequently, by largely independent behavior of aluminum on silica. In general, the evolving Al/Si-stoichiometry of colloids can be considered as evidence that colloids are formed by condensation processes. If some disintegration took place, they are not significant.

The source of the calcium in colloids could be plagioclase and possibly calcite. Despite the fact that calcite was not identified directly in primary rock, it could occur in micro-fractures of granitoid rocks (White et al., 1999). The calcite dissolution rate $\sim 10^{-5}$ mol m^{-2} s^{-1} exceeds by 7 orders of magnitude the dissolution rate of plagioclase feldspar (Plummer et al., 1978). Gaboriaud et al. (1999) and Phair and VanDeventer (2001) suggested that calcium could act as a bridge in alumina-silica polymerization, based on the hypothetical reaction scheme,

$$\equiv Si{-}O^{-} + Ca^{2+} \rightarrow \equiv Si{-}O{-}Ca^{+} \qquad (7)$$

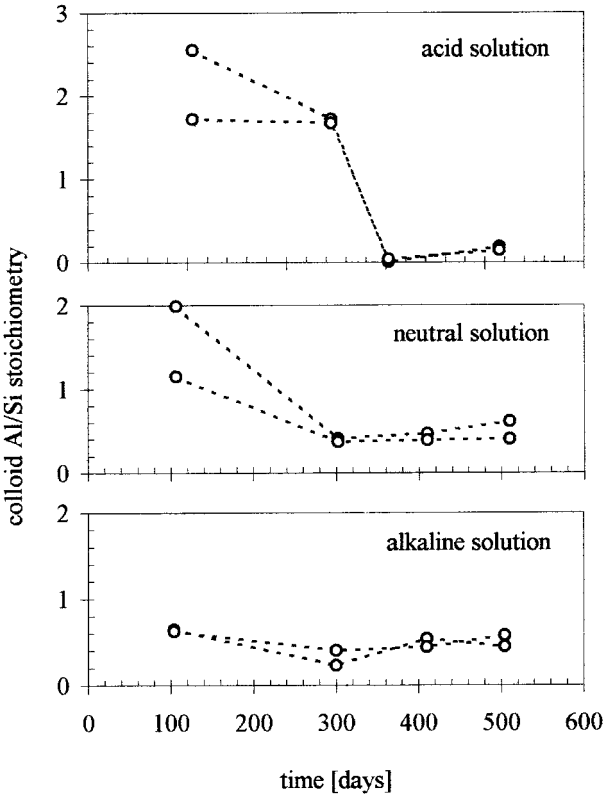

Figure 11. Evolution of the colloid Al/Si-stoichiometry.

and

$$\equiv Si-O-Ca^{+} + {}^{-}O-Al\equiv \rightarrow \equiv Si-O-Ca-O-Al\equiv. \quad (8)$$

Enhanced Ca-contents in colloid particles have been already mentioned by Degueldre and Wernli (1987) and Degueldre et al. (1989). Other elements that were concentrated in colloids (S, Cl, Ba, P) were probably either (1) sorbed on a particle surface or (2) incorporated into the structure: for example Gunnars et al. (2002) reported a high correlation between Fe and P due to the formation of basic $Fe^{(III)}$-phosphates. The enhanced contents of the former elements indicate the high capability of colloids to incorporate other components and confirm the role of colloids as pollutant "carriers" and "scavengers".

4.2.3. *Dynamics*

Total mathematic solution of the dynamic model in Figure 7 could not be accomplished because of missing data on instantaneous contents of all

aqueous components, nuclei, and secondary phases. Nevertheless, overall Al- and Si-fluxes into colloids could be calculated. The data sets (Figure 3) were regressed by polynomial functions of 2nd–4th orders. Based on the derivatives of the functions, overall fluxes of the k-component into colloids, $j^{(k)}_{o(coll)} = \sum j^{(k)}_i$ ($i = 9$–12, see the model in Figure 7), were found. Evolution of the overall Si- and Al-fluxes into colloids in time is presented in Figure 12. To balance the fluxes into and from solutions, the overall fluxes into colloids were extrapolated to zero time: They were estimated to be 1.08, 0.18, and 0.06 μmol day^{-1} of silica and 0.90, 0.42, and 0.07 μmol day^{-1} of aluminum from the alkaline, neutral and acid solutions, respectively.

The individual fluxes $j^{(k)}_5$ into nuclei and consecutively also $j^{(k)}_6$ into colloids (see model on Figure 7) should dominate over other fluxes from solution at the early stages of the experiment. Then, the total fluxes out from solution could be very roughly represented by the overall fluxes into colloids.

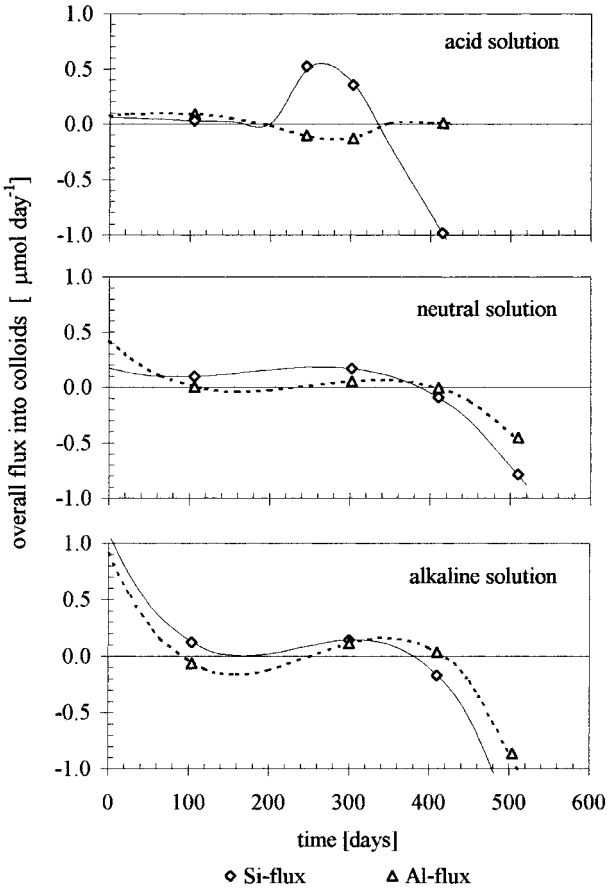

Figure 12. Evolution of the overall Si- and Al-fluxes into colloids.

Table VIII. Comparison of the overall fluxes into solutions and into colloids (μmol day^{-1})

Solution	Overall fluxes into solutions				Overall fluxes into colloids			
	Si-flux at		Al-flux at		Si-flux at		Al-flux at	
	zero time	27th day	zero time	27th day	zero time	27th day	zero time	27th day
Acid	8.2	1.63	0.76	0.21	0.06	0.05	0.07	0.09
Neutral	8.6	1.70	2.22	0.62	0.18	0.13	0.42	0.26
Alkaline	9.2	1.77	3.33	0.75	1.08	0.71	0.90	0.53

A comparison of the overall fluxes into solutions with those into colloids, both at the initial stages of the experiment, is presented in Table VIII and Figure 13. As can be seen, the proportion of the fluxes into colloids on the total fluxes increased with time and pH. The Al-fluxes into colloids participated in the total fluxes to a larger extent than the Si-fluxes. The overall fluxes into colloids approached the individual fluxes into solutions, $j_1^{(k)}$ (especially in the neutral and alkaline solutions, compare with Table VII). This indicates that the fluxes from new surfaces probably influenced (increased) the fluxes into colloids during the early stages of the experiments.

In the alkaline solutions, a high correlation ($R^2 = 0.96$) between the fluxes of colloidal Al and Si was found (Figure 14). This indicates a highly coordinate Al-Si behavior, which is consistent with the stable colloid Al/Si-stochiometry (see Figure 11). The slope of the correlation line, 0.69, is in relatively good agreement with the former estimated colloid stoichiometry. A weaker correlation ($R^2 = 0.67$) is visible in the neutral solutions due to the highest Al-fluxes at the early stages of the experiment (Figure 14). In the acid solutions, the Si-fluxes are practically independent of Al-fluxes (Figure 14), probably due to a higher affinity of aluminum to sulfates.

The question remains as to why the colloid concentrations, having reached a maximum, decreased again. No correlation between the colloid concentrations and solution superstauration was found. The *R*-squared values were substantially lower than 0.1, except for the correlation between Al-colloids and the SI with respect to gibbsite in acid solutions ($R^2 = 0.128$) and between Si-colloids and the SI with respect to kaolinite in neutral solutions ($R^2 = 0.113$). This fact indicates that the concentration of colloids was controlled by more factors than by supersaturation only. It is well known that colloid stability is sensitive to pH-changes. However, pH was very stable in all solutions after the 27th day due to buffering of rock/CO_2 system. Ionic strength, the additional factor controlling colloid stability, probably did not increase to such an extent to cause colloid aggregation. Although the ionic

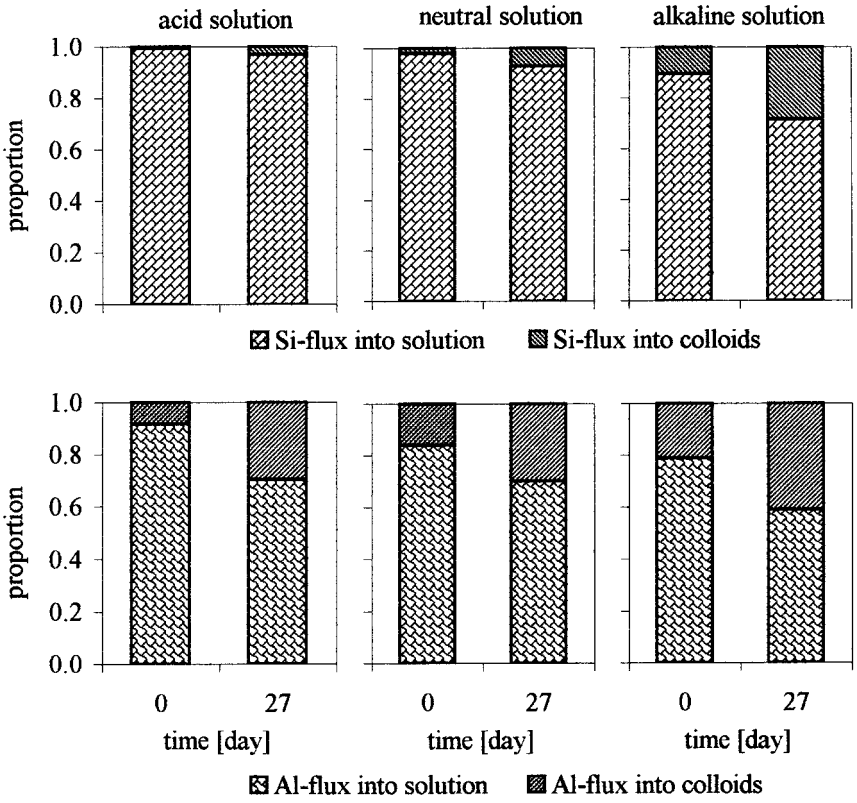

Figure 13. A comparison of the overall fluxes into solutions and into colloids at the initial stages of experiment (at zero and 27th day).

strength was not fixed at the start of the experiment, the concentrations of the ions controlling ionic strength, Na^+ and K^+ (and probably Ca^{2+} and HCO_3^- ions), quickly attained steady state and did not increase. Moreover, Na-ions in alkaline solutions evidently decreased during the experiment without any maintainence of prior colloid content. Based on geochemical modeling, maximal ionic strengths were estimated as 2×10^{-3}, 1.5×10^{-3} and 1.8×10^{-3} mol l^{-1} in the acid, neutral and alkaline solutions, respectively. Former arguments support the assumption that supersaturation, pH, and ionic strength did not control the concentration of colloids at the advanced stages of the experiment. Nevertheless, one explanation remains: the formation of colloids can be the result of a competition between homogeneous and heterogeneous phenomena. At the early stages of the experiments, as soon as certain supersaturation had been reached, the formation of a new phase was largely initiated by homogeneous nucleation (flux j_5, see Figure 7). The newly formed particles (a) grew into the macroscopic phase, aggregated and settled (flux j_7), or (b) were stabilized by a surface electric charge and,

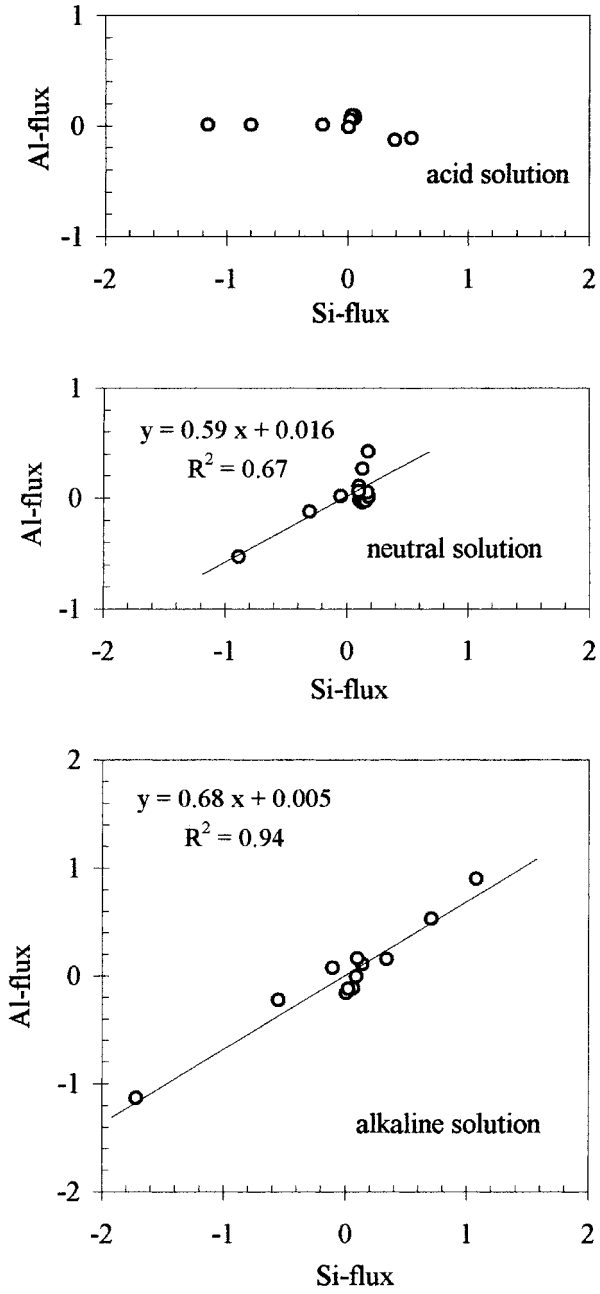

Figure 14. Correlation between the overall fluxes of colloidal Al and Si.

having been protected from colliding, they were accumulated in the solution as colloids (flux j_9). Despite relative "time stability", these colloids slowly aggregated and settled (flux j_{11}). As the surface area of the newly formed

aggregates had enlarged, the flux j_3 dominated over the flux j_5 and crystal growth dominated over nuclei (colloid) formation.

4.3. SECONDARY SOLIDS

Stoichiometry of the secondary solids isolated from the neutral solutions on the 24th day of the experiment suggests the formation of Al-hydroxides/oxides and perhaps some clay minerals, or more likely some amorphous phases (e.g., allophanes). Unfortunately, it was not possible to isolate adequate amounts of secondary phases, and thus the phases could not be analyzed by X-ray diffraction. In the secondary phases isolated from neutral and alkaline solutions after termination of the experiments (and evaporation), the slightly enhanced contents of K indicate the presence of K-mica, perhaps of illite. High contents of Mg together with Fe suggest the existence of chlorite. The low content of Na, on the other hand, questioned the expected occurrence of smectites such as Na-beidelite. X-ray diffraction confirmed chlorites and K-mica. The diaspore and quartz probably came from Al-phases formed at the early stages of the experiment and from imperfectly eliminated primary phases, respectively. Other phases, if any, were either amorphous or under the limit of detection.

In the solids isolated from acid solutions after experiments, only a relatively low content of sulfur was found, considering that the part aluminum had been expected to precipitate as sulfate. Despite these small contents, X-ray diffraction confirmed only sulfates, even if a little bit "exotic". Alternative phases expected on the basis of EDX analysis were probably of low crystallinity.

Enhanced contents of Ti, P, Cl, Ba, and S in all secondary phases perhaps came from aggregates of colloids, in which these elements were slightly concentrated.

After subtracting the normative mineral, hypothetical barite, gypsum, halite, apatite, and albite and real clinochlore, $Mg_5Al_2Si_3O_{10}(OH)_8$, the remaining contents were normalized to 10 O-atoms and 2 OH-groups to estimate the clay mineral composition. The stoichiometry determined roughly relates to illite (Table IX).

5. Conclusions

The long-term experiments confirmed that Si- and Al-colloids could be formed in *rock*-water system without any changes of conditions and fluxes from the surroundings. A high supersaturation with respect to secondary solids was reached in solutions as a consequence of dissolution and precipitation dynamics. In these conditions, new phases nucleated and condensed. Part of these phases remained dispersed in solutions as colloids. If some disintegration processes had participated, they were not significant. The formation of colloids

Table IX. Stoichiometry of the newly formed clay minerals

Solution	Composition
Acid	$K_{0.55}Ca_{0.11}Mn_{0.01}Fe_{0.51}Al_{1.31}Ti_{0.07}[Si_{4.00}O_{10}(OH)_2]$
	$K_{0.72}Ca_{0.17}Mn_{0.01}Fe_{0.51}Al_{1.40}[Al_{0.32}Ti_{0.08}Si_{3.60}O_{10}(OH)_{2]}$
Neutral	$K_{0.55}Ca_{0.11}Mn_{0.03}Fe_{0.87}Al_{1.33}[Al_{0.55}Ti_{0.05}Si_{3.40}O_{10}(OH)_2]$
	$K_{0.73}Ca_{0.06}Fe_{0.18}Al_{1.85}[Al_{0.74}Ti_{0.02}Si_{3.24}O_{10}(OH)_2]$
Alkaline	$K_{0.48}Fe_{1.37}Al_{1.07}[Al_{0.46}Ti_{0.11}Si_{3.43}O_{10}(OH)_2]$
	$K_{1.30}Ca_{0.06}Mn_{0.01}Fe_{0.25}Al_{1.38}[Al_{0.13}Ti_{0.02}Si_{3.85}O_{10}(OH)_2]$

[a]Computed from EDX analysis after subtracting normative barite, gypsum, halite, apatite, albite and clinochlore, $Mg_5Al_2Si_3O_{10}(OH)_8$.

was favored by higher pH values. The mean concentrations of the colloidal Si and Al exceeded 50 and 20 μmol l^{-1}, in both the neutral and alkaline solutions, whereas those in the acid solutions reached only 48 and 12 μmol l^{-1}, respectively. In the alkaline and neutral solutions, the colloid matter evolved in a similar way as secondary solids, in the sequence *Al-hydroxide–clay minerals*. In the acid solutions, aluminum and silica behaved broadly independently due to aluminum sulfate precipitation. The concentration of colloidal aluminum and silica increased during the first 200–400 days of the experiments, when the formation of a new phase had been initiated by homogeneous nucleation. From maximum, the content of colloids decreased to nearly zero, probably as a result of gradual aggregation and the predominant growth of new secondary solids on the surface of already formed aggregates.

The colloids formed during these experiments are mainly representative of colloid populations formed during the weathering of freshly crushed rock. They can largely be generated as the environmental impacts of various constructions or waste disposal projects (at a mine or construction sites) that have an abundance of fractured rocks.

Acknowledgements

The author gratefully acknowledges P. Kadlec, Drs. V. Vávra, M. Gregerová, and P. Sulovský for analyses, Drs. P. Vilks and J. Zeman, and two anonymous reviewers for their constructive comments.

References

Adu-Wusu K. and Wilcox W. R. (1991) Kinetics of silicate reaction with gibbsite. *J. Coll. Int. Sci.* **143**, 127–138.

Bache B. W. and Sharp G. S. (1976) Soluble polymeric hydroxy-aluminium ions in acid soils. *J. Soil Sci.* **27**, 167–174.

Benedettia M., Ranville J. F., Ponthieua M. and Pinheiroc J. P. (2002) Field-flow fractionation characterization and binding properties of paniculate and colloidal organic matter from the Rio Amazon and Rio Negro. *Organic Geochem.* **33**, 269–279.

Bottero J. Y., Cases J. M., Flessinger F. and Poirier J. E. (1980) Studies of hydrolyzed aluminum chloride solutions. 1. Nature of aluminum species and composition of aqueous solutions. *J. Phys. Chem.* **84**, 2933–2939.

Bourrié G., Grimaldi C. and Régeard A. (1989) Monomeric versus mixed monomeric–polymeric models for aqueous aluminium species: Constraints from low-temperature natural waters in equilibrium with gibbsite under temperate and tropical climate. *Chem. Geol.* **76**, 403–417.

Brandt F., Bosbach D., Krawczyk-Bärsch E., Arnold T. and Bernhard G. (2003) Chlorite dissolution in the acid pH-range: A combined microscopic and macroscopic approach. *Geochim. Cosmochim. Acta* **67**, 1451–1461.

Brantley S. L., Crane S. R., Crerar D. A., Hellmann R. and Stallard R. (1986) Dissolution of dislocation etch pits in quartz. *Geochim. Cosmochim. Acta* **50**, 2349–2361.

Browne B. A. and Driscoll C. T. (1992) Soluble aluminum silicates: Stoichiometry, stability, and implications for environmental geochemistry. *Science* **256**, 1667–1670.

Busenberg E. and Clemency C. V. (1976) The dissolution kinetics of feldspars at 25 °C and 1 atm. CO_2 partial pressure. *Geochim. Cosmochim. Acta* **40**, 41–49.

Chou L. and Wollast R. (1984) Steady-state kinetics and dissolution mechanisms of albite. *Am. J. Sci.* **285**, 963–993.

Crerar D. A., Axtmann E. V. and Axtmann R. C. (1981) Growth and ripening of silica polymers in aqueous solutions. *Geochim. Cosmochim. Acta* **45**, 1259–1266.

Degueldre C. A. and Wernli B. (1987) Characterization of the natural inorganic colloids from a reference granitic ground water. *Anal. Chim. Acta* **195**, 211–223.

Degueldre C., Baeyens B., Goerlich W., Riga J. Verbist J. and Stadelmann P. (1989) Colloids in water from a subsurface fracture in granitic rock, Grimsel Test Site, Switzerland. *Geochim Cosmochim. Acta* **53**, 603–610.

Determann H. (1967) *Gelchromatographie*. Springer Verlag, Berlin-Heidelberg-New York.

Dia A., Gruau G., Olivié-Lauquet G., Riou C., Molénat J. and Curmi P. (2000) The distribution of rare earth elements in ground waters: Assessing the role of source-rock composition, redox changes and colloidal particles. *Geochim. Cosmochim. Acta* **64,** 4131–4151.

Dietzel M. (2000) Dissolution of silicates and the stability of polysilicic acid. *Geochim. Cosmochim. Acta* **64**, 3275–3281.

Dupre B., Viers J., Dandurand J.-L., Polve M., Benezeth P., Vervier P. and Braun J.-J. (1999) Major and trace elements associated with colloids in organic-rich river waters: Ultrafiltration of natural and spiked solutions. *Chem. Geol.* **160**, 63–80.

Eggleston C. M., Hochella Jr. M. F. and Parks G. A (1989) Sample preparation and aging effects on the dissolution rate and surface composition of diopside. *Geochim. Cosmochim. Acta* **53**, 797–804.

Faimon J. (1995) *Natural Al and Si Colloids Formed During Aluminosilicate Weathering*. Ph.D. thesis. Masaryk University, Brno, Czech Republic (in Czech).

Faimon, J. (1998) Kinetics of the release of silicon and aluminium from aluminosilicates into aqueous mildly acid solutions. *Scripta Fac. Sci. Nat. Univ. Masaryk Brun.* (Brno, Czech Rep.), **25**, 59–68.

Faimon J. and Ondráček Z. (1993) Gel filtration chromatography with HF detector – a useful tool for the study of natural colloids. *Scripta Fac. Sci. Nat. Univ. Masaryk Brun.* (Brno, Czech Rep.), **23** (Geology), 3–15.

Gaboriaud, F., Nonat, A., Chaumont, D. and Craievich, A. (1999) Aggregation and gel formation in basic silico-calco-alkaline solutions studies: A SAKS, SANS and ELS study. *J. Phys. Chem. B* **103**, 5775–5781.

Gíslason S. R., Heaney P. J., Oelkers E. H. and Schott J. (1997) Kinetic and thermodynamic properties of moganite, a novel silica polymorph. *Geochim. Cosmochim. Acta* **61**, 1193–1204.

Grindrod P., Peletier M. and Takase H. (1999) Mechanical interaction between swelling compacted clay and fractured rock, and the leaching of clay colloids. *Eng. Geol.* **54**, 159–165.

Gunnars A., Blomqvist S., Johansson P. and Andersson C. (2002) Formation of Fe(III) oxyhydroxide colloids in freshwater and brackish seawater, with incorporation of phosphate and calcium. *Geochim. Cosmochim. Acta* **66**, 745–758.

Hall S. B., Duffield J. R. and Williams D. R. (1991) A reassessment of the applicability of the DLVO theory as an explanation for the Schulze–Hardy rule for colloid aggregation. *J. Coll. Int. Sci.* **143**, 411–415.

Hamilton J. P., Pantano C. G. and Brantley S. L. (2000) Dissolution of albite glass and crystal. *Geochim. Cosmochim. Acta* **64**, 2603–2615.

Hine P. T. and Bursill D. B. (1984) Gel permeation chromatography of humic acid. *Water Res.* **18**, 1461–1465.

Holdren Jr., G. R. and Adams J. E. (1982) Parabolic dissolution kinetics of silicate minerals: An artifact of nonequilibrium precipitation processes? *Geology* **10**, 186–190.

Holdren Jr., G. R. and Speyer P. M. (1985) pH dependent changes in the rates and stoichiometry of dissolution of an alkali feldspar at room temperature. *Am. J. Sci.* **285**, 994–1019.

Hunter K. A. (1983) On the estuarine mixing of dissolved substances in relation to colloid stability and surface properties. *Geochim. Cosmochim. Acta* **47**, 467–473.

Kalinowski B. E., Faith-Ell C. and Schweda P. (1998) Dissolution kinetics and alteration of epidote in acidic solutions at 25 °C. *Chem. Geol.* **151**, 181–197.

Kalinowski B. E., Liermann L. J., Brantley S. L., Barnes A. and Pantano C. G (2000) X-ray photoelectron evidence for bacteria-enhanced dissolution of hornblende. *Geochim. Cosmochim. Acta* **64**, 1331–1343.

Klepetsanis P. G. and Koutsoukos P. G. (1991) Spontaneous precipitation of calcium sulfate at conditions of sustained supersaturation. *J. Coll. Int. Sci.* **143**, 299–308.

Knauss K. G. and Wolery T. J. (1986) Dependence of albite dissolution kinetics on pH and time at 25 and 70 °C. *Geochim. Cosmochim. Acta* **50**, 2481–2497.

Kühnel R. A. (1987) The role of cationic and anionic scavengers in laterites. *Chem. Geol.* **60**, 31–40.

Lasaga A. C. (1981) Rate laws of chemical reactions. In *Kinetics of Geochemical Processes* (eds. A. C. Lasaga and R. J. Kirkpatrick), Review in Mineralogy, Vol. 8, Chap. 1, pp. 1–68. Min. Soc. Am., Chelsea, Michigan.

Lasaga A. C. and Blum A. E. (1986) Surface chemistry, etch pits and mineral/water reactions. *Geochim. Cosmochim. Acta* **50**, 2363–2379.

Lægdsmand M., Villholth K. G., Ullum M. and Jensen K. H. (1999) Processes of colloid mobilization and transport in macroporous soil monoliths. *Geoderma* **93**, 33–59.

Liermann L. J., Kalinowski B. E. Brantley S. L. and Ferry J. G. (2000) Role of bacterial siderophores in dissolution of hornblende. *Geochim. Cosmochim. Acta* **64**, 587–602.

Mackin J. E. and Aller R. C. (1984) Diagenesis of dissolved aluminium in organic rich estuarine sediments. *Geochim. Cosmochim. Acta* **48**, 299–313.

Malmström M. and Banwart S. (1997) Biotite dissolution at 25 °C: The pH dependence of dissolution rate and stoichiometry. *Geochim. Cosmochim. Acta* **61**, 2779–2799.

Mast M. A. and Drever J. I. (1987) The effect of oxalate on the dissolution rates of oligoclase and tremolite. *Geochim. Cosmochim. Acta* **51**, 2559–2568.

May H. M., Acker J. G., Smyth J. R., Bricker O. P. and Dyar M. D. (1995) Aqueous dissolution of low-iron chlorite in dilute acid solutions at 25 °C. *32nd Annual Meeting Clay Minerals Society*.

McCarthy J. F. and Shevenell L. (1998) Processes controlling colloid composition in a fractured and karstic aquifer in eastern Tennessee, USA. *J. Hydrol.* **206**, 191–218.

Means J. C. and Wijayaratne R. (1982) Role of natural colloids in the transport of hydrophobic pollutants. *Science* **215**, 968–970.

Mills W. B., Liu S. and Fong F. K. (1991) Literature review and model (COMET) for colloid/metals transport in porous media. *Ground Wat.* **29**, 199–208.

Missana T., Alonso Ú. and Turrero M. J. (2003) Generation and stability of bentonite colloids at the bentonite/granite interface of a deep geological radioactive waste repository. *J. Cont. Hydrol.* **61**, 17–31.

Moran S. B. and Moore R. M. (1989) The distribution of colloidal aluminium and organic carbon in coastal and open ocean waters off Nova Scotia. *Geochim. Cosmochim. Acta* **53**, 2519–2527.

Overbeek J. Th. G. (1977) Recent developments in the understanding of colloid stability. *J. Coll. Int. Sci.* **58**, 408–422.

Oxburgh R., Drever J. I. and Sun Y. T. (1994) Mechanism of plagioclase dissolution in acid solutions at 25 °C. *Geochim. Cosmochim. Acta* **58**, 661–669.

Parkhurst D. L. and Appelo C. A. J. (1999) User's guide to PHREEQC (Version 2) a computer program for speciation, batch-reaction, one-dimensional transport, and inverse geochemical calculations: *U.S. Geol. Surv. Water-Res. Investig. Report* 99-4259, 312 p.

Phair J. W. and VanDeventer J. S. J. (2001) Effect of silicate activator pH on the leaching and material characteristics of waste-based inorganic polymers. *Min. Engin.* **14**, 289–304.

Plummer L. N., Wigley T. M. L. and Parkhurst D. L. (1978) The kinetics of calcite dissolution in CO_2-water systems at 5–60 °C and 0.0–1.0 atm CO_2. *Am. J. Sci.* **278**, 179–216.

Pokrovsky O. S. and Schott J. (2002) Iron colloids/organic matter associated transport of major and trace elements in small boreal rivers and their estuaries (NW Russia). *Chem. Geol.* **190**, 141–179.

Pokrovski G. S., Schott J., Hazemann J.-L., Farges, F. O. and Pokrovsky O. S. (2002) An X-ray absorption fine structure and nuclear magnetic resonance spectroscopy study of gallium–silica complexes in aqueous solution. *Geochim. Cosmochim. Acta* **66**, 4203–4322.

Pokrovski G. S., Schott J., Farges F. O. and Hazemann J.-L. (2003) Iron (III)–silica interactions in aqueous solution: Insights from X-ray absorption fine structure spectroscopy. *Geochim. Cosmochim. Acta* **67**, 3559–3573.

Porcelli D., Andersson P. S., Wasserburg G. J., Ingri J. and Baskaran M. (1997) The importance of colloids and mires for the transport of uranium isotopes through the Kalix River watershed and Baltic Sea. *Geochim. Cosmochim. Acta* **61**, 4095–4113.

Puls R. W. and Powell R. M. (1992) Transport of inorganic colloids through natural aquifer material: Implications for contaminant transport. *Env. Sci. Technol.* **26**, 614–621.

Puls R. W., Eychaner J. H. and Powell R. M. (1990) Colloidal-facilitated transport of inorganic contaminants in ground water: Part I. Sampling considerations. *US Env. Prot. Agency, EPA/600/M-90/023*, 1–12.

Puls R. W., Powell R. M., Clark D. A. and Paul C. J. (1991) Facilitated transport of inorganic contaminants in ground water: Part II. Colloidal transport. *US Env. Prot. Agency, EPA/600/M-91/040,* 1–12.

Rimstidt J. D. and Barnes H. L. (1980) The kinetics of silica–water reactions. *Geochim. Cosmochim. Acta* **44**, 1683–4699.

Rochelle C. A., Bateman K., MacGregor R., Pearce J. M., Savage D. and Wetton P. D. (1996) Experimental determination of chlorite dissolution rates. *Materials Research Society Symposium*.

Rothbaum H. P. and Rohde A. G. (1979) Kinetics of silica polymerization and deposition from dilute solutions between 5 and 180 °C. *J. Coll. Int. Sci.* **71**, 533–559.

Schweda P. (1989) Kinetics of alkali feldspar dissolution at low temperature. In *Proc. 6th Int. Symp. Water/Rock Interaction* (ed. D. L. Miles), pp. 609–612. A. A. Balkema.

Shimada K. and Tarutani T. (1979) Gel chromatographic study of the polymerization of silicic acid. *J. Chrom.* **168**, 401–406.

Steefel C. I. and Van Cappellen P. (1990) A new kinetic approach to modeling water–rock interaction: The role of nucleation, precursors, and Ostwald ripening. *Geochim. Cosmochim. Acta* **54**, 2657–2677.

Steinmann P., Billen T., Loizeau J.-L. and Dominik J. (1999) Beryllium-7 as a tracer to study mechanisms and rates of metal scavenging from lake surface waters. *Geochim. Cosmochim. Acta* **63**, 1621–1633.

Stillings L. L., Drever J. I., Brantley S. L., Sun Y. T. and Oxburgh, R. (1996) Rates of feldspar dissolution at pH 3–7 with 0–8 M oxalic acid. *Chem. Geol.* **132**, 79–89.

Stumm W. and Morgan J. J. (1981) *Aquatic Chemistry*. Wiley and Sons.

Sverdrup H. U. and Warfvinge P. (1988) Weathering of primary silicate mineral in the natural soil environment in relation to a chemical weathering model. *Water Air Soil Poll.* **38**, 387–408.

Sverdrup, H. and Warfvinge, P. (1995) Estimating field weathering rates using laboratory kinetics. In *Chemical Weathering Rates of Silicate Minerals* (eds. White, A. F. and Brantley, S. L.), pp. 485–541.

Swartz C. H., Ulery A. L. and Gschwend P. M. (1997) An AEM-TEM study of nanometer-scale mineral associations in an aquifer sand: Implication for colloid mobilization. *Geochim. Cosmochim. Acta* **61**, 707–718.

Tarutani T. (1970) Chromatographic behavior of silicic acid on Sephadex columns. *J. Chrom.* **50**, 523–526.

Taylor S. T., Blum J. D., Lasaga A.C. and MacInnis I. N. (2000) Kinetics of dissolution and Sr release during biotite and phlogopite weathering. *Geoch. Cosmochim. Acta* **7**, 1191–1208.

Thornber M. R., Bettenay E. and Russell W. G. R. (1987) A mechanism of aluminosilicate cementation to form a hardpan. *Geochim. Cosmochim. Acta* **51**, 2303–2310.

Viers J., Dupré B., Polvé M., Schott J., Dandurand J.-L., and Braun J. J. (1997) Chemical weathering in the drainage basin of a tropical watershed (Nsimi-Zoetele site, Cameroon): Comparison between organic-poor and organic-rich waters. *Chem. Geol* **140**, 181–206.

Vilks P., Miller H. G. and Doern D. C. (1991) Natural colloids and suspended particles in the Whiteshell research area, Manitoba Canada, and their potential effect on radiocolloid formation. *Appl. Geoch.* **6**, 565–574.

Von Gunten H. R., Waber U. E. and Krahenbuhl U. (1988) The reactor accident at Chernobyl: A possibility to test colloid-controlled transport of radionuclides in a shallow aquifer. *J. Cont. Hydrol.* **2**, 237–247.

Waber U. E., Lienert C. and Von Gunten H. R. (1990) Colloid-related infiltration of trace metals from a river to shallow groundwater. *J. Cont. Hydrol.* **6**, 251–265.

Wada S. I. and Wada K. (1981) Reactions between aluminate ions and orthosilicic acid in dilute alkaline to neutral solutions. *Soil Sci.* **132**, 267–273.

Wegner M. W. and Christie J. M. (1983) Chemical etching of deformation substructures in quartz. *Phys. Chem. Minerals.* **9**, 67–79.

Welch S. A. and Ullman W. J. (1996) Feldspar dissolution in acidic and organic solutions: Compositional and pH dependence of dissolution rate. *Geochim. Cosmochim. Acta* **60**, 2939–2948.

Wilkinson K. J., Nègre J.-C. and Buffle J. (1997) Coagulation of colloidal material in surface waters: The role of natural organic matter. *J. Cont. Hydrol.* **26**, 229–243.

White A. F., Bullen T. D., Vivit D. V., Schulz M. S. and Clow D. W. (1999) The role of disseminated calcite in the chemical weathering of granitoid rocks. *Geochim. Cosmochim. Acta* **63**, 1939–1953.

Yamanaka C., Yokoyama T. and Tarutani T. (1986) Retarding effect of aluminium on polymerization of silicic acid particles. *J Chrom.* **367**, 419–422.

Yariv S. and Cross H. (1979) *Geochemistry of Colloid Systems*. Springer-Verlag.

Yates D. M., Joyce K. J. and Heaney P. J. (1998) Complexation of copper with polymeric silica in aqueous solution. *Appl. Geochem.* **13**, 235–241.

Yau W. W., Kirkland J. J. and Bly D. D. (1979) *Modern Size-exclusion Liquid Chromatography*. A Wiley-Interscience Publication, New York.

Yokoyama T., Yamanaka C. and Tarutani T. (1987) Formation of silicato complexes of aluminium in aqueous solution. *J. Chrom.* **403**, 151–157.

Yokoyama T., Takahashi Y. and Tarutani T. (1991) Retarding and accelerating effects of aluminum on the growth of polysilicic acid particles. *J. Coll. Int. Sci.* **141**, 559–563.

Zänker H., Moll H., Richter W., Brendler V., Hennig C., Reich T., Kluge A. and Hüttig G. (2002) The colloid chemistry of acid rock drainage solution from an abandoned Zn–Pb–Ag mine. *Appl Geochem.* **17**, 633–648.

Zhang H. and Bloom P. R. (1999) Dissolution kinetics of Hornblende in organic acid solutions. *Soil Sci. Soc. Am. J.* **63**, 815–822.